

Design of MIMO Systems with Energy Detection Receivers for Future Sub-TeraHertz Applications

Simon Bicaïs, Jean-Baptiste Doré, Valentin Savin

► **To cite this version:**

Simon Bicaïs, Jean-Baptiste Doré, Valentin Savin. Design of MIMO Systems with Energy Detection Receivers for Future Sub-TeraHertz Applications. PIMRC 2020 - IEEE International Symposium on Personal, Indoor and Mobile Radio Communications, IEEE, Aug 2020, Londres, United Kingdom. cea-03114037

HAL Id: cea-03114037

<https://hal-cea.archives-ouvertes.fr/cea-03114037>

Submitted on 18 Jan 2021

HAL is a multi-disciplinary open access archive for the deposit and dissemination of scientific research documents, whether they are published or not. The documents may come from teaching and research institutions in France or abroad, or from public or private research centers.

L'archive ouverte pluridisciplinaire **HAL**, est destinée au dépôt et à la diffusion de documents scientifiques de niveau recherche, publiés ou non, émanant des établissements d'enseignement et de recherche français ou étrangers, des laboratoires publics ou privés.

Design of MIMO Systems with Energy Detection Receivers for Future Sub-TeraHertz Applications

Simon Bicaïs, Jean-Baptiste Doré, Valentin Savin
CEA-Leti, Minatec Campus, Grenoble, France
contact: simon.bicaïs@cea.fr

Abstract—To meet the requirements of beyond 5G networks, the significant amount of unused spectrum in sub-TeraHertz frequencies is contemplated to realize high data-rate wireless communications. Yet, the performance of sub-TeraHertz systems is severely degraded by strong oscillator phase noise. Therefore, we investigate in this paper the use of multiple-inputs multiple-outputs (MIMO) systems with non-coherent detection receivers to achieve high spectral efficiency communications robust to phase noise. Based on energy detection receivers, we derive the maximum likelihood symbol detection decision rule and compare it to the standard Euclidean receiver. The performance of the detectors is assessed through numerical simulations on a realistic scenario modeling an indoor wireless link. Results demonstrate that sub-TeraHertz systems with high spectral efficiency can be implemented on low complexity and low power architectures using MIMO systems and energy detection receivers.

Index Terms—Sub-TeraHertz communications, MIMO, Amplitude modulation, Envelope detectors, Detection algorithms.

I. INTRODUCTION

With regard to the spectrum shortage in cellular bands, the interest for communications in frequencies above 90 GHz is continuously growing [1]. *Sub-TeraHertz* (sub-THz) frequencies from 90 to 300 GHz offer a significant amount of unused spectrum [2] and therefore represent a true opportunity to achieve high data-rate wireless communications. Sub-THz communication systems are considered to be one of the foremost solutions to meet the requirements of beyond-5G applications. In particular, this paper investigates one of the contemplated sub-THz scenarios [2]: an indoor high data-rate wireless link. Nonetheless, this paper provides general results relevant to other applications such as the enhanced hot-spot *kiosk* or short-range communications, *etc.*

To achieve high data-rate sub-THz communications, additional researches are required to design efficient and new physical layer algorithms. Traditional techniques cannot be directly transposed to sub-THz bands as they do not consider the unique features of radio-frequency (RF) impairments of sub-THz systems. In particular, they suffer from strong phase impairments due to the poor performance of high-frequency oscillator [2]. State-of-the-art approaches [2] investigate the use of coherent systems together with channel bonding. This type of architecture needs to be further combined with signal processing optimization to mitigate the effects of phase impairments leading to complex RF architectures. Conversely, we consider non-coherent detection for its inherent robustness to phase noise and simple implementation – already realized for sub-THz frequencies in [3] – and in particular, energy detection receivers. Transceivers based on energy detection

have been extensively studied for systems with a single transmit antenna and multiple receive antennas, see [4] and references therein. Nonetheless, it follows from non-coherent sub-THz communication systems that challenges lie in increasing spectral efficiency. With regard to this statement, the work in [5] is relevant as it shows that multi-inputs multi-outputs (MIMO) systems with amplitude detection receivers may exploit spatial multiplexing and diversity gains using multiple transmit antennas to increase their spectral efficiency. Similarly, we investigate the design of MIMO systems with energy detection receivers to achieve high spectral efficiency sub-THz communications.

This paper mainly pursues the work in [5] by evaluating communication performance in a sub-THz scenario. More precisely, we assume directive antennas and strongly correlated channels while in [5] the channel is built from i.i.d. Gaussian entries. Moreover, the envelope detection scheme in [5] is based on the amplitude detection of complex received signals, *i.e.* baseband signals from a coherent receiver. In contrast, we consider envelope extraction with energy detectors. The contributions of the paper are the following. First, we detail the system model for MIMO systems using energy detection receivers. The sub-THz propagation channel is introduced as well as the RF chains of the transmitter and receiver. Second, the design of the receiver detection algorithm is investigated. We propose and compare two detectors: the maximum likelihood (ML) detection criterion, derived upon a high signal-to-noise ratio (SNR) assumption, and the standard Euclidean decision rule. Third, we evaluate the performance of these detectors for uncoded and coded systems with numerical simulations modeling a fixed indoor wireless link in the D-band at 145 GHz. Results show that the spectral efficiency of non-coherent sub-THz systems may be efficiently increased using the combination of MIMO systems and energy detection receivers with low complexity and low power RF architectures.

The remainder of this paper is structured as follows. Sec. II outlines the system model. In Sec. III, the design of the receiver detection algorithm is addressed. Sec. IV is dedicated to numerical simulations. Eventually, potential perspectives are discussed in Sec. V while Sec. VI draws some conclusions.

II. SYSTEM MODEL

A. Transceiver description

We consider in this paper a MIMO communication system as illustrated in Fig. 1. The number of antennas is denoted N_t at the transmitter and N_r at the receiver. The propagation

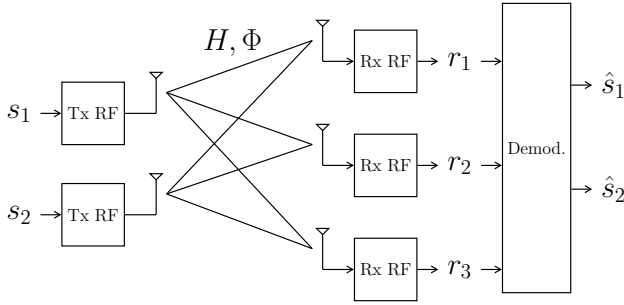


Fig. 1: Block diagram of a 2×3 MIMO transceiver

channel is described by two $N_r \times N_t$ matrices: $H = (h_{k,n})$ and $\Phi = (\varphi_{k,n})$ where $h_{k,n}^2$ and $\varphi_{k,n}$ describe respectively the propagation gain and phase shift of the channel for signals transmitted on the n -th Tx RF chain and received on the k -th Rx RF chain. To refer to this channel, we adopt hereafter the symbolic notation $n \rightarrow k$. In addition, it is of interest to express the propagation gain for channel $n \rightarrow k$ as $h_{k,n}^2 = g_{k,n}^{\text{Tx}} \cdot l_{k,n} \cdot g_{k,n}^{\text{Rx}}$ to highlight the influence of the antennas directivity gains $g_{k,n}^{\text{Tx}}$, $g_{k,n}^{\text{Rx}}$ and the path loss $l_{k,n}$. Let the column vector $\mathbf{s} = [s_1 \dots s_{N_t}]^T$ denotes the sent symbols and $\mathbf{r} = [r_1 \dots r_{N_r}]^T$ the received symbols. The transceiver uses envelope modulation at the transmitter and non-coherent demodulation at the receiver.

B. Transmitter RF chain

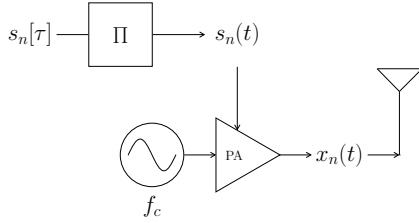


Fig. 2: Block diagram of one Tx RF chain

The transmitter implements envelope modulation and the architecture of its RF chains is depicted in Fig. 2. Using envelope modulation allows a simple implementation and an efficient use of power amplifiers. On the n -th RF chain, we write $s_n(t)$ the modulating signal which lies in $\mathbb{R}_{\geq 0}$ and results from a rectangular pulse-shaping. It is defined by

$$s_n(t) = \sum_{\tau \in \mathbb{Z}} s_n[\tau] \cdot \frac{\Pi(\frac{t}{T} - \tau)}{\sqrt{T}}, \quad t \in \mathbb{R} \quad (1)$$

where $s_n[\tau] \in \mathbb{R}_{\geq 0}$ is the τ -th modulated symbol from constellation \mathcal{C} of unit average energy and T denotes the symbol duration. It should be mentioned that $\int_{\tau}^{\tau+T} |s_n(t)|^2 dt = s_n[\tau]^2$. Then the transmitted signal $x_n(t)$ at carrier frequency f_c is expressed by :

$$x_n(t) = s_n(t) \cdot \sqrt{2} \cos(2\pi f_c t + \phi(t)), \quad (2)$$

where $\phi(t)$ is a stochastic process modeling a strong oscillator phase noise. The transmitter uses a single local oscillator reference, common to all Tx RF chains, and therefore, the phase noise process is unique.

C. Propagation channel

The recent measurement campaigns have confirmed the theoretical expectations that the line-of-sight path provides most of the energy contribution in sub-THz propagation channels. For characterization through measurements of the indoor radio propagation channel between 126 and 156 GHz, we refer the reader to [6] and to [7] for complementary results on non-line-of-sight components. Otherwise, the modeling of sub-THz channels through deterministic ray-tracing is addressed in [8]. Accordingly, we assume in this paper a static line-of-sight channel model.

D. Receiver RF chain

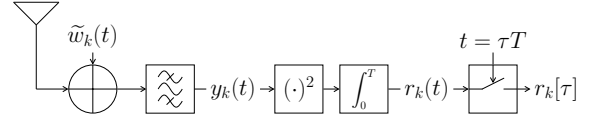


Fig. 3: Block diagram of one Rx RF chain

Let us here detail the receiver RF chains whose architecture is depicted in Fig. 3. At the entry of the k -th chain, we have the band-limited¹ signal $y_k(t)$, with bandwidth $B \geq 2/T$ centered around carrier frequency f_c . This signal is given by

$$y_k(t) = \sum_{n=1}^{N_t} h_{k,n} s_n(t) \cdot \sqrt{2} \cos(2\pi f_c t + \varphi_{k,n} + \phi(t)) + w_k(t) \cdot \sqrt{2} \cos(2\pi f_c t), \quad (3)$$

where $w_k(t)$ is a band-limited continuous Gaussian process with spectral density N_0 modeling thermal noise. The channel phase shift $\varphi_{k,n} = d_{k,n} \cdot 2\pi f_c / c$ with $d_{k,n}$ the propagation distance and c the light speed. The frequency down-conversion of the signal of interest to baseband is achieved, without impact of phase noise, by squaring signal $y_k(t)$ and low-pass filtering it. That is

$$r_k(t) = \int_t^{t+T} y_k(t)^2 dt, \quad (4)$$

with $f_c \gg 1/T$. For the k -th Rx RF chain, the τ -th received symbol $r_k[\tau]$ is obtained after integration and sampling as follows

$$\begin{aligned} r_k[\tau] &= r_k(\tau T), \\ &= \sum_{n=1}^{N_t} \sum_{m=1}^{N_t} h_{k,n} s_n[\tau] \cdot h_{k,m} s_m[\tau] \cos(\varphi_{k,n} - \varphi_{k,m}) \\ &\quad + 2 \int_{\tau T}^{\tau T+T} w_k(t) \sum_{n=1}^{N_t} h_{k,n} s_n(t) \cos(\varphi_{k,n} + \phi(t)) dt \\ &\quad + \int_{\tau T}^{\tau T+T} w_k(t)^2 dt. \end{aligned} \quad (5)$$

Regarding this equation, it is worth noting that the first term represents the energy of the received signals of the different Tx

¹The band-pass filter is required to prevent the spectral folding of noise.

RF chains whereas the two following terms express the contribution of thermal noise in the received symbols. Accordingly, we denote the energy of received signals

$$E_k[\tau] = \sum_{n=1}^{N_t} \sum_{m=1}^{N_t} h_{k,n} s_n[\tau] h_{k,m} s_m[\tau] \cos(\varphi_{k,n} - \varphi_{k,m}). \quad (6)$$

E. Probability distribution of received symbols

In this subsection, we derive the distribution of received symbols. Concerning Eq. (5), let us use the following notation

$$S_k(t) = \sum_{n=1}^{N_t} h_{k,n} s_n(t) \cos(\varphi_{k,n} + \phi(t)), \quad (7)$$

which leads to

$$\int_T S_k(t)^2 dt = \frac{E_k[\tau]}{2}. \quad (8)$$

The latter equation is obtained under a strong oscillator phase noise assumption which results in no loss of generality. With an observation of duration T , signals $S_k(t)$ and $w_k(t)$ are band-limited signals with band B , duration T and finite energy. It follows from [9] that these signals lie in a signal space of dimension² $2M = \lfloor 2BT \rfloor + 1$ and thus can be decomposed onto an orthonormal basis $\psi = \{\psi_i\}_{1 \leq i \leq 2M}$. This decomposition enables us to derive the probability distribution of received symbols and is expressed by

$$S_k(t) = \sum_{i=1}^{2M} S_k^i \cdot \psi_i(t), \quad w_k(t) = \sum_{i=1}^{2M} w_k^i \cdot \psi_i(t). \quad (9)$$

The scalar coefficients of the decomposition verify

$$\sum_{i=1}^{2M} |S_k^i|^2 = \int_T S_k(t)^2 dt = \frac{E_k[\tau]}{2}, \quad (10)$$

$$\mathbb{E} \left[\sum_{i=1}^{2M} |w_k^i|^2 \right] = \mathbb{E} \left[\int_T w_k(t)^2 dt \right] = N_0 B, \quad (11)$$

where $\mathbb{E}[\cdot]$ is the expectation operator. Therefore, coefficients w_k^i are zero-mean Gaussian variables with variance $\sigma_w^2 = N_0 B / 2M$. By definition of basis ψ , we have $\int_T \psi_i(t) \psi_j(t) dt = \delta_{ij}$. We are now in a position to express the distributions of the integrals in Eq. (5) as

$$\begin{aligned} \int_T w_k(t) S_k(t) dt &= \sum_{i=1}^{2M} \sum_{j=1}^{2M} w_k^i S_k^j \int_T \psi_i(t) \psi_j(t) dt \\ &= \sum_{i=1}^{2M} w_k^i S_k^i \sim \mathcal{N} \left(0, \frac{E_k[\tau]}{2} \cdot \sigma_w^2 \right), \end{aligned} \quad (12)$$

and

$$\begin{aligned} \int_T w_k(t)^2 dt &= \sum_{i=1}^{2M} \sum_{j=1}^{2M} w_k^i w_k^j \int_T \psi_i(t) \psi_j(t) dt \\ &= \sum_{i=1}^{2M} (w_k^i)^2 \sim \sigma_w^2 \cdot \chi_{2M}^2. \end{aligned} \quad (13)$$

²In the considered scenario, we have $2M = 5$.

In summary, the received symbols are given by

$$r_k[\tau] = E_k[\tau] + \sqrt{\frac{E_k[\tau]}{M}} \cdot \sum_{i=1}^{2M} w_k^i + \sum_{i=1}^{2M} |w_k^i|^2, \quad (14)$$

where $w_k^i \sim \mathcal{N}(0, \sigma_w^2)$ are zero-mean Gaussian variables with variance $\sigma_w^2 = N_0 B / 2M$. From now on, the time index τ is disregarded for brevity.

III. DETECTION ALGORITHM DESIGN

A. Maximum likelihood detector (MLD)

It is known [10] that for independent and equiprobable symbols the ML decision rule is the optimum detection criterion *i.e.* minimizing the symbol error rate (SER). The ML criterion is defined upon the channel likelihood function by

$$\hat{s} = \arg \max_{s \in \mathcal{C}^{N_t}} p(\mathbf{r} | \mathbf{s}, H, \Phi). \quad (15)$$

With regard to Eq. (14), the expression of the channel likelihood function involves an integration over the whole probability space due to the superposition of χ^2 and Gaussian distributions. The resulting detection criterion would be too complex to be evaluated in practical systems. Nonetheless, under a high SNR assumption, the variance of the χ^2 distribution is close to zero. In order to derive an analytical decision rule, we pursue the analysis under this assumption and model the χ^2 contribution by its expected value. It follows that the received symbol r_k is distributed according to

$$r_k \sim \mathcal{N}(\mu_k, \sigma_k^2), \quad (16)$$

where the mean and variance are given by

$$\mu_k = E_k + 2M \cdot \sigma_w^2, \quad (17)$$

$$\sigma_k^2 = 2E_k \cdot \sigma_w^2 + \varepsilon. \quad (18)$$

The definition of E_k is given in Eq. (6). The term ε is introduced to prevent discontinuity³ in the detection criterion. Then, the joint probability density function is expressed by

$$p(\mathbf{r} | \mathbf{s}, H, \Phi) = \prod_{k=1}^{N_r} \frac{1}{\sqrt{2\pi\sigma_k^2}} \exp \left(-\frac{|r_k - \mu_k|^2}{2\sigma_k^2} \right). \quad (19)$$

Finally, the ML decision rule is written as

$$\hat{s} = \arg \min_{s \in \mathcal{C}^{N_t}} \sum_{k=1}^{N_r} \frac{|r_k - \mu_k(\mathbf{s})|^2}{\sigma_k(\mathbf{s})^2} + \ln(\sigma_k(\mathbf{s})^2). \quad (20)$$

The latter equation fully describes the *maximum likelihood detector* further abbreviated by *MLD*. Though the minimization space \mathcal{C}^{N_t} is exponential in N_t , the constellation \mathcal{C} used by the system should not present a high modulation order. For this reason, the complexity of the MLD algorithm is not an issue. It must be emphasized that the MLD requires the estimation of H and Φ and thus the implementation of an estimation algorithm. The estimation of H and Φ exceeds the scope of this paper and hence is not presented. In the following, we assume perfect knowledge of the channel at the receiver.

³Empiric results have shown that setting $\varepsilon = \sigma_w^2$ is an efficient choice to minimize the SER.

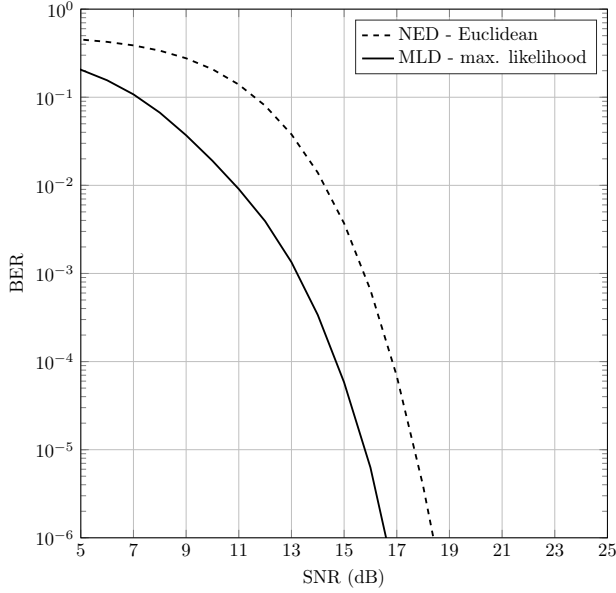


Fig. 4: Receivers performance for systems without spatial interference and using OOK

B. Naive Euclidean detector (NED)

We present in this paragraph the *naive Euclidean detector (NED)*. This detection criterion is inherited from the assumption that symbols are transmitted over perfectly spatially multiplexed Gaussian channels with no inter-antennas interference, *i.e.* H is diagonal. Under this hypothesis, the NED is the optimum decision rule defined by the standard Euclidean distance minimization,

$$\hat{s}_k = \arg \min_{s \in \mathcal{C}} |r_k - h_{k,k}^2 s^2|. \quad (21)$$

This detection criterion estimates symbol \hat{s}_k on the k -th Rx RF chain. This detector is interesting to consider as it does not require the estimation of the phase shift matrix Φ but only the propagation gains $h_{k,k}^2$. In addition, this receiver presents a low complexity as it demodulates symbols from the different Rx RF chains independently and leads to a simple implementation.

IV. NUMERICAL SIMULATIONS

A. MIMO case without spatial interference

To compare the different detectors, we first investigate MIMO systems without spatial interference. The channels are perfectly spatially multiplexed, *i.e.* H is diagonal. This case enables us to evaluate the performance of the detectors regarding the channel described in Eq. (14). To complete the scenario description, the modulation scheme used by the transceiver is On-Off Keying (OOK) such that $\mathcal{C} = \{0, \sqrt{2}\}$. Thereon, Fig. 4 presents the results of numerical simulations for any systems with $N_t = N_r$. The performance of the detectors is expressed in terms of bit-error-rate (BER) as a function of the SNR defined by $h_{k,k}^2/\sigma_w^2$. It is shown that the MLD outperforms the NED. The MLD capitalizes on the knowledge of the channel and therefore exhibits a detection gain.

TABLE I: Simulation parameters

Parameters	Notation	Values
Carrier frequency	f_c	145 GHz
Bandwidth	$B = 2/T$	2 GHz
Thermal noise	N_0	-174 dBm/Hz
Noise figure	N_f	10 dB
Antenna gain	g_0	32 dBi
Beam width	θ	3 °
Side lobe level	ϵ	-20 dB
Distance Tx - Rx	d_0	10 m
Antenna transmit power	$P_{A_{Tx}}$	-

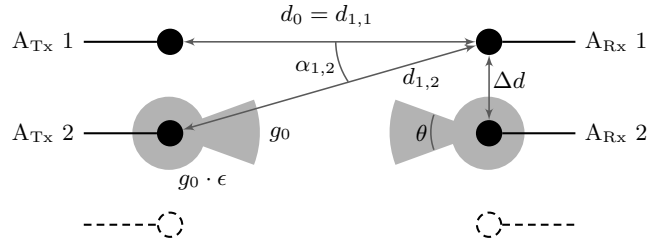


Fig. 5: Disposition of the antennas in the considered scenario

B. Scenario description: fixed indoor link in the D-band

In this paragraph, we introduce a realistic sub-THz scenario. The targeted application is a fixed indoor high data-rate wireless link in the D-band. Table I outlines the main simulation parameters for this scenario while Fig. 5 illustrates its geometry. An $N \times N$ MIMO system is considered with uniform linear arrays of antennas whose disposition is depicted in Fig. 5. The specification of the antenna is extracted from [11] which describes the design of a high-gain antenna for the D-band with transmit-arrays and PCB technology. The propagation gain $h_{k,n}^2/\sigma_w^2$ for channel $n \rightarrow k$ may be evaluated from the budget link given by the Friis' transmission equation:

$$\frac{h_{k,n}^2}{\sigma_w^2} = P_{A_{Tx}} \cdot G_{k,n} \cdot \left(\frac{c}{4\pi f_c d_{k,n}} \right)^2 \cdot \left(\frac{N_0 B}{2M} \cdot N_f \right)^{-1}, \quad (22)$$

where $G_{k,n}$ and $d_{k,n}$ stand respectively for the antennas gains and the propagation distance. We have $G_{k,n} = g_{k,n}^{Tx} \cdot g_{k,n}^{Rx}$ the product of the Tx and Rx antennas directivity gains for channel $n \rightarrow k$. We assume the commonly used sectored antenna model. The fixed antenna directivity gain is then defined by

$$g(\theta, \alpha) = \begin{cases} g_0, & \text{if } |\alpha| < \frac{\theta}{2}, \\ g_0 \cdot \epsilon, & \text{otherwise,} \end{cases} \quad (23)$$

upon the beam width θ , the beam offset angle to the main lobe α , the side lobe level ϵ ($0 < \epsilon \ll 1$) and the antenna gain g_0 . The considered scenario is symmetric and the beam of the k -th transmit antenna is aligned with the k -th receive one. This leads to $g_{k,n}^{Tx} = g_{k,n}^{Rx} = g(\theta, \alpha_{k,n})$ with $\alpha_{k,n}$ the beam offset angle for channel $n \rightarrow k$. Eventually, the channel matrix H may be evaluated with Eq. (22) from Table I and matrices $(\alpha_{k,n})$ and $(d_{k,n})$. The maximum propagation gain is $h_{k,k}^2$,

achieved for any channel $k \rightarrow k$. For an antenna transmit power $P_{A_{Tx}} = -30$ dBm, we have

$$\text{SNR} = \frac{h_{k,k}^2}{\sigma_w^2} \simeq 16.23 \text{ dB}. \quad (24)$$

With $k' \neq k$, the interference terms (off-diagonal elements) in matrix H are approximately

$$\frac{h_{k,k'}^2}{h_{k,k}^2} \simeq \begin{cases} -0.01 \text{ dB}, & \text{if } |\alpha_{k,k'}| < \frac{\theta}{2}, \\ -40.02 \text{ dB}, & \text{otherwise.} \end{cases} \quad (25)$$

It should be mentioned that the differences in path loss between channels are close to zero (< 0.02 dB for $N = 8$) when $\Delta d \ll d_0$. Subsequently, the interference level between two channels only results from the sector of the antennas. Under the condition $\Delta d \geq d_0 \tan(\frac{\theta}{2})$, the antennas are almost perfectly spatially multiplexed as the interference follows from side lobes of the antennas, and hence, is very low (< -40 dB). This corresponds closely to an ideal case and the performance of the transceivers for any N equals the one described by the MIMO case without spatial interference in Fig. 4. Nevertheless, the latter condition entails a large spatial occupation ℓ , the width of the receiver and the transmitter, since $\Delta d > 26$ cm. Considering a uniform linear array of 8 antennas, we have $\ell = (N-1)\Delta d > 1.8$ m. We thus consider in the following subsection the case where one antenna beam enlightens several receive antennas to reduce Δd and hence the spatial occupation ℓ .

C. MIMO case with spatial interference

In order to reduce the spatial occupation, we consider in this paragraph the condition $\Delta d \geq \frac{2}{\kappa+1}d_0 \tan(\frac{\theta}{2})$, defined upon parameter $\kappa \in \{1, 3, \dots, 2N-1\}$. From a physical aspect, this condition expresses the case where one transmit antenna beam enlightens up to κ receive antennas. By way of illustration, the channel propagation gain matrix for $\kappa = 3$ could be accurately approximated by

$$H = \begin{bmatrix} 1 & 1 & \rho & \dots & \rho \\ 1 & 1 & 1 & \dots & \vdots \\ \rho & 1 & 1 & \dots & \rho \\ \vdots & \vdots & \vdots & \ddots & \vdots \\ \rho & \dots & \rho & 1 & 1 \end{bmatrix}. \quad (26)$$

This matrix is defined by two parameters⁴: κ denoting the number of diagonals whose elements are 1 and ρ modeling the residual interference due to side lobes of the antennas with $\rho^2 = -40$ dB. Let us now evaluate the influence of κ on communications through numerical simulations. In these simulations, the propagation gain and phase shift matrices are not approximated and are exactly computed from the scenario description and simulation parameters outlined in Sec. IV-B. The results of numerical simulations are depicted in Fig. 6. The BER performance is outlined for $N = 8$ and different values of κ . The properties exhibited in Fig. 6 also hold for different values of N . First, it must be noted

⁴The differences in path loss between channels is less than 0.02 dB such that the adjacent channels interference and the residual side lobes interference can be respectively approximated to 1 and a constant ρ .

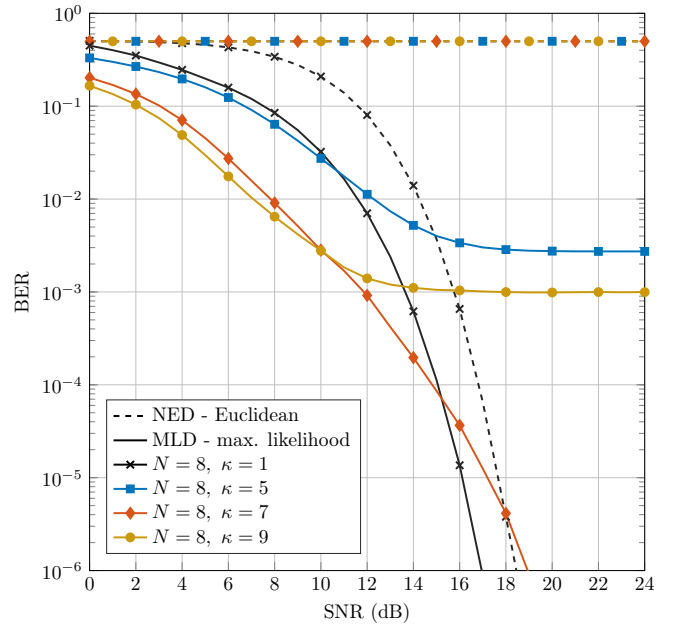


Fig. 6: Influence of κ on performance for $N = 8$

that the MLD is essential to communicate on correlated channels with spatial interference since the NED presents a BER of $1/2$ for any $\kappa > 1$. Further, it is shown that setting $\kappa = 1$ is optimal, yet $\kappa = N - 1$ is an interesting choice to achieve low error rate communications with a reduced spatial occupation. Simulation results also show that, in the moderate SNR regime, transceivers with high values of κ may demonstrate lower BER than the optimal case $\kappa = 1$. With channel coding, such property may be beneficial for configurations with κ large. If the BER is low enough, the waterfall feature of the decoding algorithm may be exhibited at a lower SNR.

Further, it is interesting to consider the integration of a forward error correction (FEC) scheme to achieve channel coding gain and low packet error rates (PER). The simulated PER with channel coding have been obtained by Monte-Carlo simulations and are reported in Fig. 7 for different N . The presented values of κ correspond, for each N , to the one demonstrating the best PER performance. The FEC scheme is a polar code with a packet size of 4096 bits, a coding rate of $9/10$ and using a successive cancellation decoder. The probabilistic bit values at the input of the channel decoder are evaluated upon the MLD decision rule. Results confirm the aforementioned property that systems with high values of κ can outperform the perfectly multiplexed systems *i.e.* $\kappa = 1$, up to a 4 dB gain for an 8×8 system. Subsequently, it is shown that an 8×8 MIMO system may communicate over 10 m in the D-band with a PER inferior to 10^{-4} , an antenna transmit power $P_{A_{Tx}} \leq -37$ dBm and a spatial occupation $\ell \leq 37$ cm. The data-rate of the system is 7.2 Gbit/s for a 2 GHz band which results in a spectral efficiency of $\eta = 3.6$ bit/s/Hz. It should be noticed that the data-rate is evaluated for a channel of 2 GHz bandwidth. Thereupon, a channel bounding scheme

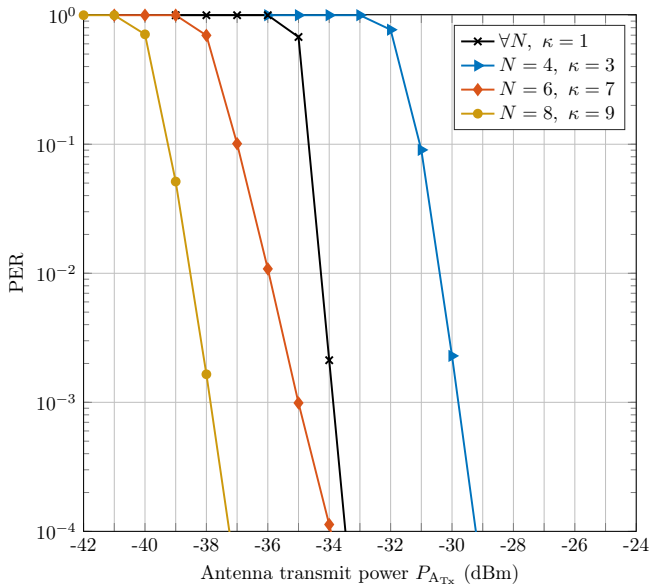


Fig. 7: PER performance for polar coded systems with coding rate 9/10 and OOK modulation scheme

could increase the aggregated throughput and allow to benefit from the large available free spectrum offered in the sub-THz bands. It can be concluded that MIMO systems using energy detection receivers may achieve high spectral efficiency wireless communications in sub-THz bands with low power and low complexity RF architectures.

Regarding short-range communications, it is worth mentioning a different numerical application where simulation parameters remain the same but $d_0 = 50$ cm. It results that a spatial occupation $\ell \leq 1.8$ cm and an antenna transmit power $P_{A_{Tx}} \leq -62$ dBm ensure a PER inferior to 10^{-4} .

V. PERSPECTIVES

In this section, we intend to provide the readers with some of the potential perspectives to this work. First, we consider evaluating a neural-network based demodulation. The use of a neural network is motivated by the non-linear multi-variable features of the channel described in Eq. (14) which could be, *a fortiori*, efficiently estimated by a neural network. Besides, the fixed property of the indoor wireless link is suited for machine learning. Results of numerical simulations with a neural network based receiver are promising. Nonetheless, the integration of a FEC is, in this case, problematic since the evaluation of probabilistic bit values is unclear and yet to be addressed. Second, the probabilistic bit values derived from the MLD decision rule present significant differences in terms of protection depending on the transmit antenna and on the transmitted symbol. A joint modulation and channel coding design optimization (*e.g.* similar to multi-level coding techniques) could exploit the latter property to further enhance demodulation performance. Third, it is of practical interest to characterize and compare the robustness of the different detectors to imperfect RF components. In particular, envelope detectors based on diodes may present non-ideal square law response such that $X_{out} \propto X_{in}^\alpha$ with $\alpha < 2$ [12].

VI. CONCLUSION

In this paper, we have investigated the design of MIMO systems with energy detection receivers for future application in sub-THz bands. We have first described the system model by characterizing the sub-THz propagation channel and the RF architectures of the transmitter and receiver. Next, we have derived upon this model the maximum likelihood decision rule, optimum for symbol detection under a high SNR assumption. This detector has been compared to the standard Euclidean detector. Later, a realistic scenario modeling an indoor high data-rate wireless link has been considered to assess by numerical simulations the performance of these detectors. It has been proved that the maximum likelihood detection is necessary to achieve low error rate communication on correlated channels with spatial interference. Furthermore, we have shown that polar-coded MIMO systems with spatial interference may exhibit performance gains in comparison to the spatial interference free case, up to a 4 dB gain for an 8×8 antennas configuration. In conclusion, results demonstrate that MIMO systems with energy detection receivers offer a valuable solution to achieve high spectral efficiency sub-THz communications with low power and low complexity RF architectures.

REFERENCES

- [1] T. S. Rappaport, Y. Xing, O. Kanhere, S. Ju, A. Madanayake, S. Mandal, A. Alkhateeb, and G. C. Trichopoulos, "Wireless Communications and Applications Above 100 GHz: Opportunities and Challenges for 6G and Beyond," *IEEE Access*, vol. 7, pp. 78 729–78 757, 2019.
- [2] J.-B. Doré, Y. Corre, S. Bicaïs, J. Palicot, E. Faussurier, D. Kténas, and F. Bader, "Above-90GHz Spectrum and Single-Carrier Waveform as Enablers for Efficient Tbit/s Wireless Communications," in *25th International Conference on Telecommunications (ICT'2018)*, Saint-Malo, France, Jun. 2018.
- [3] J. Park, S. Kang, S. V. Thyagarajan, E. Alon, and A. M. Niknejad, "A 260 GHz fully integrated CMOS transceiver for wireless chip-to-chip communication," in *2012 Symposium on VLSI Circuits (VLSIC)*, June 2012, pp. 48–49.
- [4] L. Jing, E. De Carvalho, P. Popovski, and A. O. Martinez, "Design and Performance Analysis of Noncoherent Detection Systems With Massive Receiver Arrays," *IEEE Transactions on Signal Processing*, vol. 64, no. 19, pp. 5000–5010, Oct 2016.
- [5] G. K. Psaltopoulos and A. Wittneben, "Diversity and spatial multiplexing of MIMO amplitude detection receivers," in *2009 IEEE 20th International Symposium on Personal, Indoor and Mobile Radio Communications*, Sep. 2009, pp. 202–206.
- [6] L. Pometcu and R. D'Errico, "Characterization of Sub-THz and mmWave Propagation Channel for Indoor Scenarios," in *12th European Association on Antennas and Propagation (EurAAP 18)*, Apr 2018.
- [7] L. Pometcu and R. D'Errico, "Channel Model Characteristics in D-Band for NLOS Indoor Scenarios," *2019 13th European Conference on Antennas and Propagation (EuCAP)*, pp. 1–4, 2019.
- [8] G. Gougeon, Y. Corre, and M. Z. Aslam, "Ray-based Deterministic Channel Modelling for sub-THz Band," in *2019 IEEE International Symposium on Personal, Indoor and Mobile Radio Communications (PIMRC)*, Sep. 2019.
- [9] P. Dollard, "On the time-bandwidth concentration of signal functions forming given geometric vector configurations," *IEEE Transactions on Information Theory*, vol. 10, no. 4, pp. 328–338, October 1964.
- [10] T. Moon and W. Stirling, *Mathematical Methods and Algorithms for Signal Processing*. Prentice Hall, 2000.
- [11] F. F. Manzillo, A. Clemente, and J. L. Gonzalez-Jiménez, "High-gain D-band Transmitarrays in Standard PCB Technology for Beyond-5G Communications," *IEEE Transactions on Antennas and Propagation*, pp. 1–1, 2019.
- [12] Agilent technologies, Inc., "Square Law and Linear Detection," Application Note 986, Tech. Rep., 1999.